Expertise
and insight
for the future

Please cite the original version:

Kullaa, J. (2021). Time-Domain Damage Detection of Structures with Complex Modes Under Variable Environmental Conditions Using Bayesian Virtual Sensors. Paper presented at 8th Workshop on Civil Structural Health Monitoring. Naples. 2021.

10.1007/978-3-030-74258-4_58

Time-Domain Damage Detection of Structures with Complex Modes under Variable Environmental Conditions Using Bayesian Virtual Sensors

Jyrki Kullaa

Metropolia University of Applied Sciences, P.O. Box 4071, 00079 Metropolia, Finland
jyrki.kullaa@metropolia.fi

Abstract. A time-domain algorithm for damage detection is introduced. It is based on hardware redundancy in which the number of sensors is greater than the number of excited modes plus the number of environmental variables. Therefore, for a structure with complex modes, the minimum number of sensors is expected to be higher than that of the same structure with real modes. A two-step detection algorithm is proposed. First, the accuracy of each sensor is increased by Bayesian virtual sensing. Second, the signal of each sensor is estimated using the remaining sensors utilizing a correlation model of the training data under different environmental conditions. The residual is used to detect damage. The algorithm was studied in a numerical experiment of a frame structure having a discrete damper element, which resulted in complex mode shapes. A comparison was made with the same structure having real modes due to proportional damping. The performance of damage detection was higher with real modes and virtual sensors outperformed the raw measurements. Damage localization was also relatively successful revealing the region close to the actual damage.

Keywords: Complex Modes, Virtual Sensing, Environmental Effects, Damage Detection, Hardware Redundancy, Time-Domain Structural Health Monitoring.

1 Introduction

Structural health monitoring (SHM) utilizes sensor data to get an early warning of structural failure. Vibration-based SHM is a non-destructive technique, in which damage can be detected remotely from the sensors. Damage detection can be approached using time-domain or feature-domain techniques. In this paper, time-domain data analysis is studied. It is assumed that a sensor network is installed on the structure. Training data are needed from an undamaged structure under different environmental or operational conditions. With the proposed approach it is possible to take into account the influences of the environmental or operational variability [1]. The excitation or the environmental or operational variables are not measured.

In the data analysis for damage detection, each sensor reading is estimated using the data from the remaining sensors. Therefore, the sensor network has to be redundant. The required number of sensors in the network depends on the number of active modes as well as the number of environmental or operational variables. Generally, the mode shapes are complex due to viscous damping. Only in a special case of proportional damping the modes are real.

For under-critical damping, at each natural frequency there exist two complex conjugate modes. The response can be expressed using mode superposition. This means that the response, which is a real number, is expressed with twice the number of terms compared to the case with real modes.

A two-step algorithm is proposed for damage detection [2]. First, noise reduction is performed applying Bayesian virtual sensing to the measurement data. This is an important step, because according to detection theory, the probability of detection depends on the signal-to-noise ratio (SNR) [3]. The result of the first step is virtual sensors that are more accurate than the corresponding physical sensors. Second, applying a correlation model of the training data, each (virtual) sensor is estimated using the remaining (virtual) sensors in the network resulting in a residual vector. The residual is the difference between the (virtual) sensor reading and the corresponding estimate and its increase beyond a threshold is an indication of damage.

This paper is organized as follows. Complex modes are introduced in Section 2. Bayesian virtual sensors are derived in Section 3. The proposed algorithm for damage detection is presented in Section 4. A numerical experiment comparing damage detection with real or complex modes using either physical or virtual sensors is studied in Section 5. Finally, concluding remarks are given in Section 6.

2 Complex Modes

Complex modes occur if damping is non-proportional. Then, the real modal matrix cannot diagonalize the damping matrix and the equations of motion remain coupled. Highly complex modes can occur for example, if there exist discrete damper elements.

Starting with the second order equation of motion

$$\mathbf{m}\ddot{\mathbf{u}} + \mathbf{c}\dot{\mathbf{u}} + \mathbf{k}\mathbf{u} = \mathbf{f}(t) \tag{1}$$

where **m**, **c**, and **k** are respectively the mass, damping, and stiffness matrix of the structure, $\mathbf{u} = \mathbf{u}(t)$ is the displacement vector, $\mathbf{f}(t)$ is the load vector, and t is time. Eq. (1) can be written in a state space form, resulting in a first-order differential equation

$$\begin{bmatrix} -\mathbf{k} & \mathbf{0} \\ \mathbf{0} & \mathbf{m} \end{bmatrix} \begin{Bmatrix} \mathbf{u} \\ \ddot{\mathbf{u}} \end{Bmatrix} + \begin{bmatrix} \mathbf{0} & \mathbf{k} \\ \mathbf{k} & \mathbf{c} \end{bmatrix} \begin{Bmatrix} \mathbf{u} \\ \dot{\mathbf{u}} \end{Bmatrix} = \begin{Bmatrix} \mathbf{0} \\ \mathbf{f}(t) \end{Bmatrix} \tag{2}$$

or

$$\mathbf{M}\dot{\mathbf{x}} + \mathbf{K}\mathbf{x} = \mathbf{F}(t) \tag{3}$$

where $\mathbf{x}(t) = [\mathbf{u} \quad \dot{\mathbf{u}}]^T$ is the state vector and **M**, **K**, and **F**(*t*) are defined by the above equations. The objective is to derive a truncated mode superposition solution to Eq. (3) and study the vector space of the response. The eigenvalue analysis of Eq. (3) is first performed resulting in eigenvalues λ_r that are complex for underdamped modes, and negative real numbers for overdamped modes. Also the mode shapes are complex for underdamped modes, and real for overdamped modes. The complex eigenvalues and mode shapes exist in conjugate pairs, because the response **x**(*t*) must be real. Therefore, for each natural frequency, there exist two modes. The eigenvalues are related to the natural frequencies ω_r and modal damping ζ_r by

$$\lambda_r = -\omega_r \zeta_r \pm i\omega_r \sqrt{1-\zeta_r^2} \tag{4}$$

Eqs. (3) can be made independent with the transformation

$$\mathbf{x}(t) = \sum_{s=1}^{2N} \phi_s q_s(t) \approx \sum_{s=1}^{2n} \phi_s q_s(t) \tag{5}$$

where N is the number of degrees-of-freedom (DOF) in the finite element model, $n << N$ is the number of active modes, ϕ_s is the mode shape vector, and $q_s(t)$ the modal, or generalized, coordinate of mode *s*.

Substituting Eq. (5) into Eq. (3), multiplying with ϕ_r^T from the left, and taking into account the orthogonality of the eigenvectors [4], results in

$$\phi_r^T \mathbf{M} \phi_r \ddot{q}_r(t) + \phi_r^T \mathbf{K} \phi_r q_r(t) = \phi_r^T \mathbf{F}(t) \tag{6}$$

or

$$m_r \ddot{q}_r(t) + k_r q_r(t) = \phi_r^T \mathbf{F}(t) \tag{7}$$

which is the equation of motion for mode *r*, where $m_r = \phi_r^T \mathbf{M} \phi_r$ is the modal mass and $k_r = \phi_r^T \mathbf{K} \phi_r$ is the modal stiffness, which are generally complex. There are $2N$ such single-degree-of-freedom equations, one for each mode. In the truncated model, it is assumed that only the $2n$ lowest modes correspond significantly to the response. The solution $q_r(t)$ for Eq. (7) can be found analytically or numerically.

Let us assume that solution $q_r(t)$ is available. It depends on the loading and the initial conditions. In the underdamped case, the solutions exist in complex conjugate pairs, for example for the first two modes:

$$\begin{aligned} q_1(t) &= q_{1R}(t) + q_{1I}(t)i \\ q_2(t) &= \bar{q}_1(t) = q_{1R}(t) - q_{1I}(t)i \end{aligned} \tag{8}$$

Their contribution to the physical response according to Eq. (5) is

$$\begin{aligned}\mathbf{x}(t) &= \psi_1 q_1(t) + \psi_2 q_2(t) \\ &= \psi_1 q_1(t) + \bar{\psi}_1 \bar{q}_1(t) \\ &= \psi_1 [q_{1R}(t) + q_{1I}(t) i] + \bar{\psi}_1 [q_{1R}(t) - q_{1I}(t) i] \\ &= (\psi_1 + \bar{\psi}_1) q_{1R}(t) + (\psi_1 - \bar{\psi}_1) q_{1I}(t) i \\ &= 2\,\mathrm{Re}\,\psi_1 q_{1R}(t) - 2\,\mathrm{Im}\,\psi_1 q_{1I}(t)\end{aligned} \tag{9}$$

which shows that the solution **x**(t) lies in a space spanned by vectors $\mathrm{Re}\,\psi_1$ and $\mathrm{Im}\,\psi_1$. Therefore, the dimension of the vector space is two. In other words, two basis vectors are needed to describe the physical response if the active mode is complex.

On the other hand, if damping is zero, the eigenvalues and modes are purely imaginary, resulting in response

$$\mathbf{x}(t) = -2\,\mathrm{Im}\,\psi_1 q_{1I}(t) \tag{10}$$

In this case the solution **x**(t) lies in a space spanned by vector $\mathrm{Im}\,\psi_1$ only. The dimension of the vector space is one.

With overdamped modes, the eigenvalues and modes are real, and the response is

$$\mathbf{x}(t) = \psi_1 q_{1R}(t) \tag{11}$$

In this case the solution **x**(t) lies in a space spanned by vector ψ_1 only. The dimension of the vector space is one.

3 Bayesian Virtual Sensing

Virtual sensing (VS) gives an estimate of a quantity of interest using the available measurements. The objective of this study is to design virtual sensors that are more accurate than the hardware [1]. Empirical virtual sensing is applied, and no mathematical model of the structure is needed. In addition, the excitation is not measured or estimated. Hardware redundancy is assumed with a sufficiently large number of sensors measuring the response of the structure.

Consider a sensor network measuring p simultaneously sampled responses $\mathbf{y} = \mathbf{y}(t)$ at time instant t. The measurement **y** includes a measurement error $\mathbf{w} = \mathbf{w}(t)$:

$$\mathbf{y} = \mathbf{x} + \mathbf{w} \tag{12}$$

where $\mathbf{x} = \mathbf{x}(t)$ are the true values of the measured degrees of freedom. The objective is to find an estimate of the true values **x** utilizing the noisy measurements **y** from the sensor network. Eq. (12) can be written in the following form at each time instant t [5].

$$\begin{Bmatrix}\mathbf{x} \\ \mathbf{y}\end{Bmatrix} = \begin{bmatrix}\mathbf{I} & \mathbf{0} \\ \mathbf{I} & \mathbf{I}\end{bmatrix} \begin{Bmatrix}\mathbf{x} \\ \mathbf{w}\end{Bmatrix} \tag{13}$$

For simplicity but without loss of generality, assume zero-mean variables **x** and **y**. The partitioned covariance matrix is:

$$\begin{aligned}\boldsymbol{\Sigma} &= \mathrm{E}\left(\begin{Bmatrix}\mathbf{x}\\ \mathbf{y}\end{Bmatrix}\begin{bmatrix}\mathbf{x}^T & \mathbf{y}^T\end{bmatrix}\right) = \begin{bmatrix}\boldsymbol{\Sigma}_{xx} & \boldsymbol{\Sigma}_{xy}\\ \boldsymbol{\Sigma}_{yx} & \boldsymbol{\Sigma}_{yy}\end{bmatrix}\\ &= \begin{bmatrix}\mathbf{I} & \mathbf{0}\\ \mathbf{I} & \mathbf{I}\end{bmatrix} E\left(\begin{Bmatrix}\mathbf{x}\\ \mathbf{w}\end{Bmatrix}\begin{bmatrix}\mathbf{x}^T & \mathbf{w}^T\end{bmatrix}\right)\begin{bmatrix}\mathbf{I} & \mathbf{0}\\ \mathbf{I} & \mathbf{I}\end{bmatrix}^T\\ &= \begin{bmatrix}\mathbf{I} & \mathbf{0}\\ \mathbf{I} & \mathbf{I}\end{bmatrix}\begin{bmatrix}\boldsymbol{\Sigma}_{xx} & \mathbf{0}\\ \mathbf{0} & \boldsymbol{\Sigma}_{ww}\end{bmatrix}\begin{bmatrix}\mathbf{I} & \mathbf{I}\\ \mathbf{0} & \mathbf{I}\end{bmatrix}\\ &= \begin{bmatrix}\boldsymbol{\Sigma}_{xx} & \boldsymbol{\Sigma}_{xx}\\ \boldsymbol{\Sigma}_{xx} & \boldsymbol{\Sigma}_{xx}+\boldsymbol{\Sigma}_{ww}\end{bmatrix}\end{aligned} \tag{14}$$

where E(·) denotes the expectation operator and the measurement error **w** is assumed to be zero mean Gaussian, independent of **x**, with a (known) covariance matrix $\boldsymbol{\Sigma}_{ww}$. The covariance matrix $\boldsymbol{\Sigma}_{xx}$ is not known, but $\boldsymbol{\Sigma}_{yy}$ can be estimated from the measurement data, and if the noise covariance matrix can be approximated, then the following estimate applies: $\boldsymbol{\Sigma}_{xx} = \boldsymbol{\Sigma}_{yy} - \boldsymbol{\Sigma}_{ww}$. In this study, the measurement errors are assumed uncorrelated between sensors resulting in a diagonal noise covariance matrix. In addition, because $\boldsymbol{\Sigma}_{xx}$ must be positive definite, an upper bound of the noise level in each sensor can be derived [1].

A linear minimum mean square error (MMSE) estimate for $\mathbf{x}\,|\,\mathbf{y}$ (**x** given **y**) is obtained by minimizing the mean-square error (MSE) [5]. The expected value, or the conditional mean, of the predicted variable is:

$$\hat{\mathbf{x}} = E(\mathbf{x}\,|\,\mathbf{y}) = \boldsymbol{\Sigma}_{xx}(\boldsymbol{\Sigma}_{xx}+\boldsymbol{\Sigma}_{ww})^{-1}\mathbf{y} = \boldsymbol{\Sigma}_{xx}\boldsymbol{\Sigma}_{yy}^{-1}\mathbf{y} \tag{15}$$

and the estimation error is

$$\mathrm{cov}(\mathbf{x}\,|\,\mathbf{y}) = \boldsymbol{\Sigma}_{xx} - \boldsymbol{\Sigma}_{xx}(\boldsymbol{\Sigma}_{xx}+\boldsymbol{\Sigma}_{ww})^{-1}\boldsymbol{\Sigma}_{xx} = \boldsymbol{\Sigma}_{xx} - \boldsymbol{\Sigma}_{xx}\boldsymbol{\Sigma}_{yy}^{-1}\boldsymbol{\Sigma}_{xx} \tag{16}$$

4 Damage detection

Residual generation is an integral part of damage detection. The residual can be defined as a difference between the actual and estimated data:

$$\mathbf{r} = \mathbf{y} - \hat{\mathbf{y}} \tag{17}$$

where **y** represents either the physical or virtual sensors, $\hat{\mathbf{y}}$ is the estimate of the sensor reading obtained as follows.

Each sensor in turn is estimated using the remaining sensors in the network by applying the MMSE estimation [2]. The measured response **y** is partitioned into observed variables **v** and estimated variables **u** (typically a single sensor *u*):

$$\mathbf{y} = \begin{Bmatrix} \mathbf{y}_u \\ \mathbf{y}_v \end{Bmatrix} \tag{18}$$

For simplicity but without loss of generality, assume zero-mean variables $\mathbf{y}$. The data covariance matrix $\mathbf{S}_y$ is estimated using the training data consisting of several measurements under different environmental or operational conditions.

$$\mathbf{\Sigma}_y = E(\mathbf{y}\mathbf{y}^T) = \begin{bmatrix} \mathbf{\Sigma}_{y,uu} & \mathbf{\Sigma}_{y,uv} \\ \mathbf{\Sigma}_{y,vu} & \mathbf{\Sigma}_{y,vv} \end{bmatrix} \tag{19}$$

Similarly to the previous section, a linear minimum mean square error (MMSE) estimate for the conditional mean of $\mathbf{y}_u \mid \mathbf{y}_v$ is obtained by minimizing the mean-square error (MSE):

$$\hat{\mathbf{y}}_u = E(\mathbf{y}_u \mid \mathbf{y}_v) = \mathbf{\Sigma}_{y,uv}\mathbf{\Sigma}_{y,vv}^{-1}\mathbf{y}_v \tag{20}$$

and the MSE is

$$\text{cov}(\mathbf{y}_u \mid \mathbf{y}_v) = \mathbf{\Sigma}_{y,uu} - \mathbf{\Sigma}_{y,uv}\mathbf{\Sigma}_{y,vv}^{-1}\mathbf{\Sigma}_{y,vu} \tag{21}$$

The residual for the sensor u is then generated:

$$\mathbf{r}_u = \mathbf{y}_u - E(\mathbf{y}_u \mid \mathbf{y}_v) \tag{22}$$

Once damage occurs, the correlation structure does not fit the experimental data producing a larger residual, which will then trigger an alarm.

Residuals are standardized according to the training data. Principal component analysis (PCA) is applied to all data, and the first principal component (PC) is only retained indicating the direction with the largest change in the data space. The one-dimensional PC score vector of the residuals is then subjected to statistical analysis.

The PC scores are divided into batches of d data points. Extreme value distributions are estimated both for the block minima and block maxima of the training data [6, 7]. The extreme values are plotted on a control chart [8] with corresponding control limits. The control limits are computed for a specified probability of exceedance. In the present study, the subgroup size of d = 100 and the probability of exceedance of 0.001 were used. If the plotted data points exceed the control limits, an alarm is triggered indicating possible damage.

5 Numerical Experiment

A numerical experiment was performed to investigate damage detection of a structure having real or complex modes.

The structure was a two-dimensional steel frame (Fig. 1) with a height of 4.0 m and a width of 3.0 m. Both columns were fixed at the bottom. The frame was also supported with a horizontal spring and a discrete viscous damper at an elevation of

2.75 m with a spring constant of k = 2.0 MN/m and viscous damping coefficient of c = 11 kNs/m. For the structure with real modes, the discrete damper was absent. The frame was modelled with 44 simple beam elements with equal lengths of 250 mm and a square hollow section of 100 mm ´ 100 mm ´ 5 mm.

The lowest natural frequencies and the corresponding damping ratios of the undamaged structure with real or complex modes under nominal environmental condition were computed using Eq. (4) and are listed in Table 1. Notice that all modes were underdamped and in the case of complex modes there were two complex modes for each natural frequency. Modal damping was the only source of damping for real modes, whereas for the complex modes damping was composed both of the discrete damper and modal damping.

Horizontal random loading was applied to the right column at elevations of 4 m, 3 m, and 2 m (Fig. 1). The loads $F_1(t)$, $F_2(t)$, and $F_3(t)$ were mutually independent. The maximum frequency of the excitation was 50 Hz.

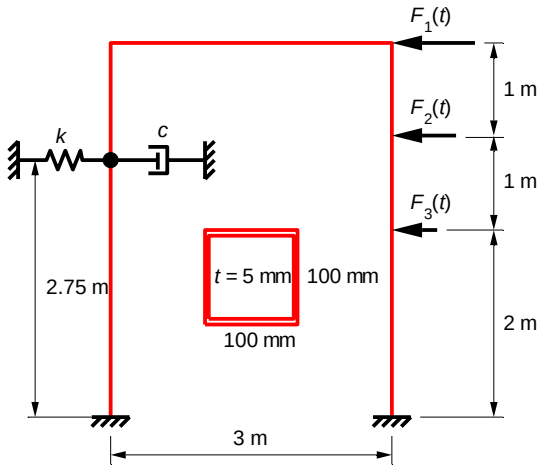

Fig. 1. Steel frame.

Table 1. Seven lowest natural frequencies and damping ratios of the two structures.

Mode number	Real modes f_n (Hz)	z	Complex modes f_n (Hz)	z
1	13.9257	0.0100	14.2361	0.0828
2	37.3384	0.0100	39.0230	0.0453
3	50.2279	0.0150	54.3517	0.3515
4	59.8129	0.0200	58.6689	0.0322
5	112.6560	0.0200	110.0559	0.2782
6	120.1176	0.0200	113.0101	0.0209
7	167.8757	0.0200	166.2691	0.0317

Steady state analysis with modal superposition was applied to compute the response of the structure. Periodic pseudorandom excitations in the frequency range between 0 and 50 Hz with random amplitudes and phases were generated [9], and the analysis was performed in the frequency domain [4]. Seven lowest modes were included in the analysis.

The analysis period was 4.096 s with a time increment of 4 ms resulting in 1024 data points. Transverse accelerations were measured with 43 sensors located at the nodes of the FE model. Gaussian noise was added to each sensor. The average SNR was 30 dB and noise standard deviations were equal in all sensors. For validation and comparison, exact transverse accelerations were also recorded.

A relatively complex environmental model was applied. The temperature of the left corner, T_{17} varied randomly between –25°C and +40°C. The subscript 17 indicates the node number. The temperature of the other end points varied randomly: $T_{29} = T_{17} \pm 5$°C; $T_1 = T_{17} \pm 3$°C; and $T_{45} = T_{29} \pm 3$°C. Temperature variation between the aforementioned points was linear. The relationship between temperature and the Young's modulus, E, was stepwise linear as shown in Fig. 2a. Sample distributions of the Young's modulus in the elements are plotted in Fig. 2b. Within each short measurement, the distribution did not change.

Due to the temperature effect, the natural frequencies varied between measurements. Fig. 3a shows the frequency variation for the structure having real modes, while Fig. 3b shows the frequency variation for the structure having complex modes. The data points to the right of the dashed vertical lines are from the damaged structure. Visually, it is difficult to detect damage from the frequency changes due to the strong environmental effect.

Damage was removal of material inside a beam element due to corrosion. The damaged element was located at the bottom of the left leg. Five different damage levels were considered with the wall thicknesses of 4.5, 4.0, 3.5, 3.0, and 2.5 mm. Notice that as the material was removed, both the stiffness and mass were decreased.

The first 40 measurements were taken from the undamaged structure and each damage level was monitored with two measurements. Training data were the first 20 measurements. The extreme value statistics (EVS) control charts were designed using the same training data.

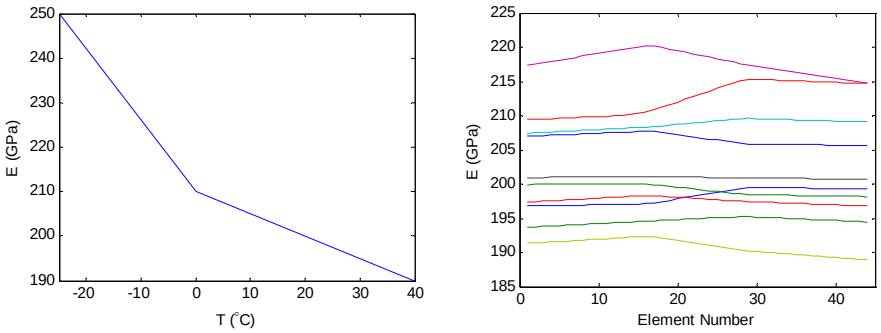

Fig. 2. (a) Young's modulus versus temperature. (b) Sample distributions of the Young's modulus.

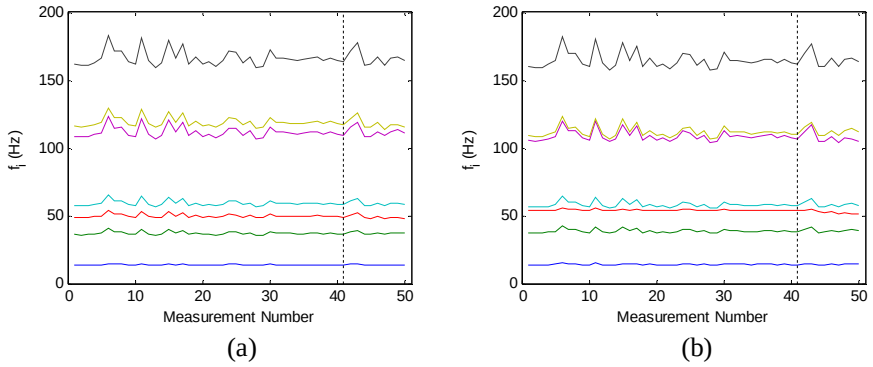

Fig. 3. Variation of the seven lowest natural frequencies due to temperature and damage for the structure with (a) real modes and (b) complex modes.

5.1 Dimensions of the data space

Studying first the noiseless response in a single measurement with constant environment, the data matrix consisted 1024 data points from 43 accelerometers. The rank of the data matrix was 7 if the modes were real, and 14 if the modes were complex. These observations support the discussion in Section 2. When noise was present and several measurements were included with different environmental conditions, full rank data matrices resulted with either model. Even in a noiseless case, the data matrix had a full rank, because the complex relationship between temperature and Young's modulus could not be completely eliminated using linear MMSE.

5.2 Damage detection

Fig. 4 shows the SNR of each physical sensor and the corresponding virtual sensor for both models. It can be seen that the SNRs of the virtual sensors were always larger than those of the hardware. Due to different acceleration levels at different regions of

the structure, the SNRs varied considerably. In particular, damage was located in a region with a low SNR (closest to sensor 1).

The residuals were first subjected to principal component analysis. The first PC scores were only retained, and the PC scores of the training data were used to identify the probability density functions (PDF) of the extreme values. Separate PDFs for the minima and maxima (or negative maxima) were identified using a subgroup size of 100. The histograms of the minima and negative maxima for the complex mode case are plotted in Fig. 5 together with the fitted PDFs. It can be seen that the theoretical PDFs closely agree with the data. Similar results were obtained for the real mode case.

EVS control charts for the first PC scores of the residual with a subgroup size of 100 are shown in Fig. 6 for real modes and in Fig. 7 for complex modes. Control charts were plotted both for the actual measurement data (left) and virtual sensor data (right). The leftmost vertical line corresponds to the end of training data, and the other vertical lines indicate the five damage levels. It can be seen that the virtual sensors were capable of detecting smaller damage than the physical sensors in both models. This is because virtual sensors had a larger SNR than the physical sensors.

For the structure with real modes, three largest damage levels were detected using the physical measurements, whereas with virtual sensors, all five damage levels could be detected. For a structure with complex modes, damage detection missed all damage levels if physical measurements were used, whereas with virtual sensors, the four largest damage levels could be detected. Damage detection with complex modes was therefore more difficult than with real modes in this particular case. Similar results were obtained if damage was located at the bottom of the right leg. Quite surprisingly, the results were similar also in the case with no environmental effects. The noise effect was probably more significant compared to the remaining environmental influences that could not be eliminated.

5.3 Damage localization

Damage was assumed to locate in the vicinity of the sensor with the largest Mahalanobis distance (MD) [10] of the residual, Eq. (22). The MDs of the residuals for each sensor are plotted both for the structure with real modes (Fig. 8a) and complex modes (Fig. 8b). In both cases, damage was localized to sensor 3 that was relatively close to the actual damage location. The closest sensor was sensor 1. The inaccuracy in damage localization was probably due to the low SNR of sensors 1 and 2, which were closer to damage than sensor 3.

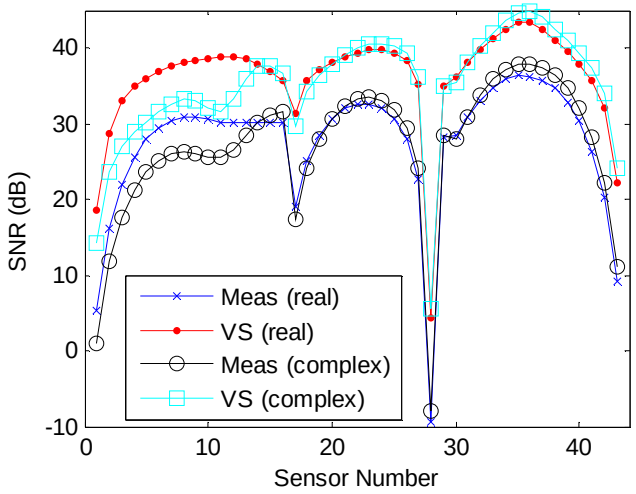

Fig. 4. SNR of raw data and the corresponding virtual sensors from the structure with real modes or complex modes.

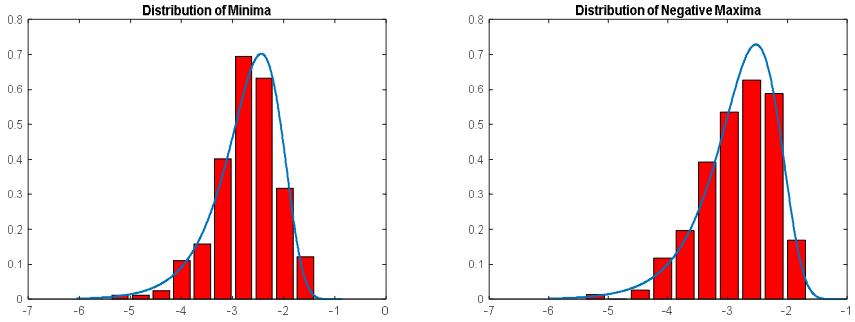

(a) (b)

Fig. 5. Identified EVS distributions and histograms for the first PC scores of the residual of the training data: (a) minima, (b) negative maxima. The data were from the structure with complex modes.

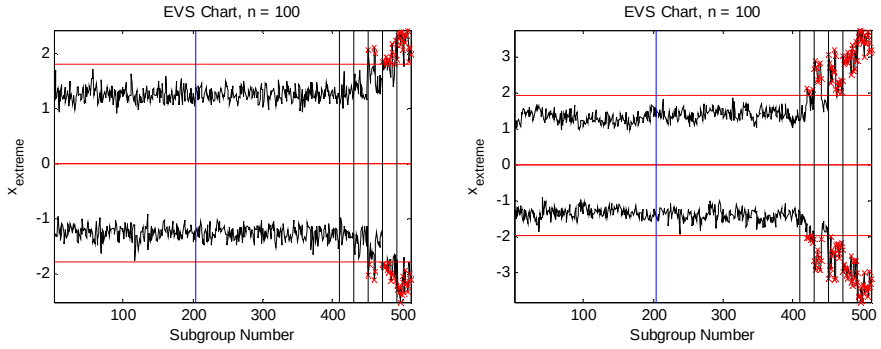

(a) (b)

Fig. 6. Damage detection for the structure with real modes: (a) raw data, (b) virtual sensors.

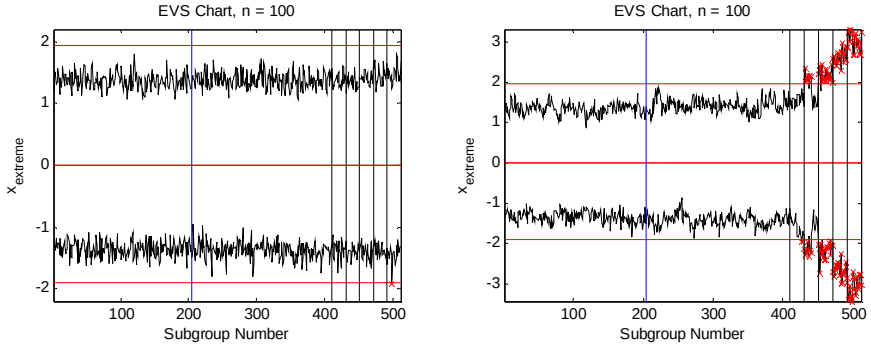

(a) (b)

Fig. 7. Damage detection for the structure with complex modes: (a) raw data, (b) virtual sensors.

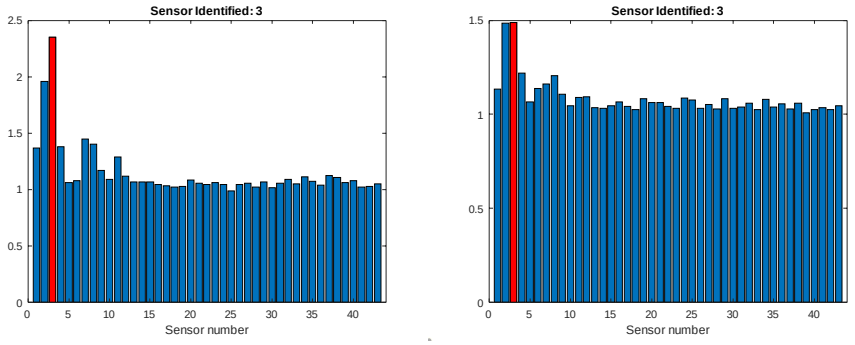

(a) (b)

Fig. 8. Damage localization using virtual sensors: (a) real modes, (b) complex modes. The actual location of damage was close to sensor 1.

6 Conclusion

Damage detection of structures having complex modes was studied. Data analysis was made directly in the time domain. A redundant sensor network with a large number of sensors was assumed. Detection performance was compared using physical or virtual sensors. In addition, the same structure with real modes was analyzed. It was shown that virtual sensors outperformed the corresponding hardware, because the SNR of the virtual sensors was higher than that of the physical sensors. Damage detection was easier for a structure with real modes than for a similar structure with complex modes. The main conclusion is that for the same detection performance in the time domain, a structure with complex modes must be equipped with a larger number of sensors than the same structure having real modes. Damage localization performance was similar in both cases revealing the region where inspection could be concentrated. The localization did not, however, result in the closest sensor to damage. An experimental study is still needed to verify the findings made in this paper.

Acknowledgement

This work was supported by Metropolia University of Applied Sciences.

References

1. Kullaa, J.: Bayesian virtual sensing in structural dynamics. Mechanical Systems and Signal Processing 115 (2019), 497–513 (2018).
2. Kullaa, J.: Robust damage detection using Bayesian virtual sensors. Mechanical Systems and Signal Processing 135 (2020), 106384 (2019).
3. Kay, S.M.: Fundamentals of statistical signal processing. Detection theory. Prentice-Hall, Upper Saddle River, NJ (1998).
4. Clough, R.W., Penzien, J.: Dynamics of structures. 2nd edn. McGraw-Hill, New York (1993).
5. Scharf, L.L.: Statistical signal processing: detection, estimation, and time series analysis. Addison-Wesley, Reading, MA (1991).
6. Coles, S.: An introduction to statistical modeling of extreme values. Springer, Bristol (2001).
7. Worden, K., Allen, D., Sohn, H., Farrar, C.R.: Damage detection in mechanical structures using extreme value statistics. SPIE Proceedings, Vol. 4693, 9th Annual International Symposium on Smart Structures and Materials, San Diego, CA, 289–299 (2002).
8. Montgomery, D.C.: Introduction to statistical quality control. 3rd edn. Wiley, New York (1997).
9. Brandt, A.: Noise and vibration analysis: signal analysis and experimental procedures. Wiley, Chichester; Hoboken, N.J. (2011).
10. Bishop, C.M.: Pattern recognition and machine learning, Springer, New York, 2006.